

Advanced SWIR sensor development at SUI

Krishna Linga^{*a}, Wei Huang^a, Bill Gustus^a, James Chi^a, John Liobe^a

^aSensors Unlimited Inc. (a wholly owned subsidiary of RTX), 330 Carter Rd, Suite 100, Princeton, NJ 08540

ABSTRACT

Sensors Unlimited Inc. (SUI), a Raytheon Company, continues to expand its sensor portfolio through the development of time-of-flight (TOF) capable technologies. The utility of SWIR for active TOF solutions is of particular interest due to its inherent eye safety characteristic. SUI is developing TOF technologies both at the detector and readout integrated circuit (ROIC) layers of the focal plane array (FPA). In this work, SUI will offer updates to the internal development efforts comprising both areas as it pertains to the time-of-flight technologies.

In this work, SUI presents an update on PIN Photodiode Array (PDA) developments and the advancements in Avalanche Photodetectors (APD) Array development. SUI continue to push the PIN based SWIR photodetector performance by reducing the dark current, increasing the quantum efficiency in broad spectral wavelength range from 400nm to 1700nm and extending the wavelength to 2.6 μ m. We will also present APD technology advancements specifically related to low temperature performance from room temperature to 260K and Geiger Mode operation. In addition, we will discuss the requirements of Readout Integrated Circuits (ROIC) for APD based sensor development for synchronous and asynchronous pulse detection and active and passive quenching mechanisms. We will also discuss 2-D and 3-D TCAD simulation results at low temperature and compare them with measured performance results. Finally, recent results related to the advanced development of Geiger Mode Avalanche Photodetectors (GMAPD) and the results using passive and active quenching circuits are presented.

Keywords: GMAPD, LMAPD, APD, SPAD, TOF, LADAR, InGaAs, SWIR

1. INTRODUCTION

This work present updates to SUI's InP based p-type, intrinsically un-doped, n-type doped (PIN) PDA designs, including improvements in fabrication processes that enable junction shape, and the photodetector designs and fabrication process improvements to achieve low dark current, high quantum efficiency and low capacitance that have been discussed extensively earlier [1, 2, 3, 4]. SUI has further designed, developed, and demonstrated trench isolation techniques to reduce the crosstalk and improve the modulation transfer function (MTF) performance for both SWIR and NIR-SWIR epitaxial structures.

SUI's SWIR FPAs have demonstrated in-pixel multimode capabilities [5, 6, 7]. One such mode of operation is range finding or time-of-flight. High resolution range finding is increasingly becoming vital functionality in high precision targeting systems. The precision and accuracy of range-to-target information is an essential performance parameter of these systems. With the recent advances in LADAR technology and sensors, range measurement accuracies as small as a centimeter have become realizable.

SUI is developing large format, high-speed, SWIR FPAs to meet the increasing field-of-view (FOV) and fast response time requirements of laser pulse detection and imaging applications, including for LADAR. For photon-starved, long-range applications, the development of large format APD-based SWIR FPAs is also ongoing.

1.1 PIN Photodetector Design

This paper summarizes the impact of the critical control factors on photodetector performance by targeting low device dark current, and low capacitance [8, 9]. The fabrication processes for these high-performance photodetector arrays have been described in detail previously [8-10]. Figure 1 shows SUI's InP/InGaAs PIN photodetector device structure, which consists of an epitaxially grown intrinsic InGaAs absorption layer, and an InP cap layer on a highly doped n-type indium phosphide (InP) substrate. The photodiodes can be fabricated for either frontside or backside illumination.

This document does not include any export controlled technical data. | CLS 45139187 | RTX, Raytheon Technologies proprietary.

*krishna.linga@rtx.com

Discrete photodiodes and linear arrays are generally front side illuminated, while 2-D arrays are backside illuminated due to the indium-based bump-bonding process used to integrate the PDA with a CMOS ROIC. The photodetector devices are fabricated using a planar fabrication process in which the individual photodiodes are planar. The cathode contact was formed around the periphery of the photodetector array by etching the epitaxial layers to make contact to the substrate. The PDAs were then flip chip bonded to a ROIC.

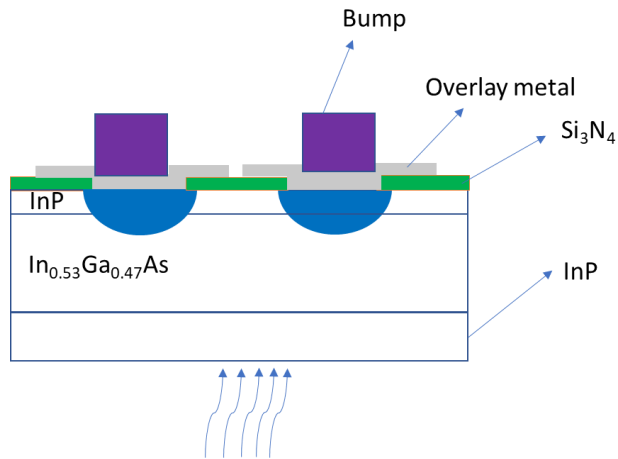


Figure 1. InP/InGaAs PIN photodiode device cross-section.

InP/InGaAs PIN photodetectors and avalanche photodetectors (APDs) have been widely used in fiber optic communication systems, 3-D LADAR imaging, free space optical communications, and other systems. With the advances in epitaxial growth of compound semiconductors using Metal Organic Chemical Vapor Deposition (MOCVD) and Molecular Beam Epitaxy (MBE) methods, there is an increasing interest in large format PIN and APD detector arrays in the shortwave infrared (SWIR) wavelength range.

In this article, we present a planar InP/InGaAs PIN and avalanche photodetector structures designed to manufacture large format focal plane arrays (FPAs) using matured fabrication technologies. As discussed above, InP PIN photodiodes consist of planar InGaAs absorption layer and a wide bandgap cap layer to reduce the surface leakage current. The APD design consists of planar InP/InGaAs avalanche photodetector structure employing n-InP multiplication layer for relatively easy fabrication with no guard ring. Other device structures such as super lattice, staircase, multi-quantum well and I²E device structures have been considered to reduce excess noise factor and increase the gain-bandwidth product, but their practical use has also been limited due to difficulties associated with the fabrication processes [11, 12, 13].

In this work, we demonstrate the design, simulation, epitaxial growth, fabrication, and characterization of state of the art InP/InGaAs APD arrays [14, 15].

1.2 Time-of-flight ROIC technology

A TOF laser system with a 2-D Focal Plane Array (FPA) is a solution for the real-time imaging, since this system can measure the TOF of multiple points in the scene instantaneously. In a direct, 2-D TOF system one can measure range by flashing the scene using a single pulse transmission without any scanning. This improves the target identification and discrimination latency while reducing overall system complexity. In these active imaging systems, also known as flash laser detection and ranging (LADAR) technology, both range and return intensity at the pixel level can be facilitated with a single laser pulse. In this way, accurate 3-D image rendering is possible with only one frame by combining the spatially and temporally coherent range and intensity data.

In general, for improving the accuracy or range of 3-D LADAR systems requires an eye safe (> 1.2 μm wavelength) laser source. Typical systems require TOF performance with resolutions on the orders of centimeters with ranges greater than 1 km. Without using GmAPD detectors or sophisticated laser scanning systems, this translates to minimum acceptable return pulse intensities on the order of 100's of photons.

This document does not include any export controlled technical data. | CLS 45139187 | RTX, Raytheon Technologies proprietary.

Additionally, with proper considerations a ROIC can be designed to offer both standard low-voltage detector biasing for low-noise imaging operation as well as linear mode avalanche operation for improved ranging performance. The ability to integrate with GMAPDs requires a full modification of the ROIC architecture and, therefore, is not amenable to agile development of multi-mode EOIR systems that include TOF capabilities. Table 1 below summarizes key performance metrics that drive SUI’s TOF-capable ROIC design.

Table 1. TOF sensor key specifications.

Nominal operating temperature	300K
Array size	640 X 512 or 1280X1024
Pixel pitch	$\geq 10 \mu\text{m}$
Minimum return pulse level	100 photons
Well capacity	$> 1\text{E}6$ electrons
Ranging scene depth	10’s 1000’s of meters
Ranging resolution	cm’s (min)
Modes of operation	Standard low-noise imaging, Asynchronous Laser Pulse Detection (ALPD), and TOF

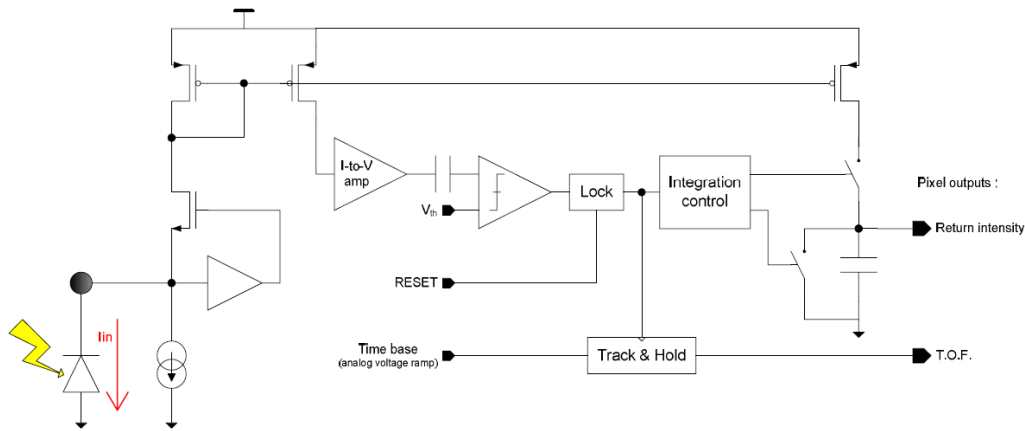


Figure 2. BDI-based TOF-capable pixel architecture.

Based on these requirements, one possible ROIC pixel architecture that can realize TOF, asynchronous laser pulse detection (ALPD), and imaging functions is shown in Figure 2 [16]. This pixel architecture utilizes a buffered direct injection (BDI) input stage with an embedded detector biasing scheme allowing for both low-noise operation and linear mode avalanche operation. The input current is mirrored and fed to a current-to-voltage amplifier. This stage performs dynamic amplification of the input current pulse. It uses capacitive coupling techniques to provide positive feedback at high frequency and thus offers high dynamic gain. This enables fast pulse detection even for low input level. Then, a high-pass filter shapes the signal at the comparator input. This pixel architecture using dynamic amplification and high pass filtering to provide robust pulse detection by triggering on a signal’s edge rather than level.

A copy of the input current is provided by another branch of the current mirror. This current is integrated on a capacitor to get the intensity of the reflected laser pulse. The integration is triggered by the pulse detection signal and is controlled by a specific stage. This stage defines a short adjustable integration window, allowing the system to consider only the useful reflected signal and not the background signal. With this pixel structure, the linearity of the intensity output is somewhat affected by the dynamic response of the input stage and an intrinsic offset current.

This document does not include any export controlled technical data. | CLS 45139187 | RTX, Raytheon Technologies proprietary.

2. BACKGROUND

2.1 Principles of operation of InGaAs APDs

APDs are semiconductor diodes (p-n junctions) which use a high internal electric field in order to cause impact ionization of electrons and holes. Impact ionization, the inverse of the Auger process, is when a carrier gains enough energy to create a secondary electron hole pair. The impact ionization process can be described as depending only on the local electric field, with the generation rate per centimeter for electrons (α) and holes (β) fitting the forms [17]:

$$\alpha(E) = \alpha_0 \exp(-[c_n/E]^{m_n}) \quad (1)$$

$$\beta(E) = \beta_0 \exp(-[c_p/E]^{m_p}) \quad (2)$$

The above rates can be derived theoretically from first principles based on the band structure [18-21], but in practice the coefficients are fitted to experimental data [22-24]. Note that the rates are also an implicit function of temperature; as the temperature is reduced, energy loss to phonon scattering is less, which increases the ionization rate [25].

Both electrons and holes can go through impact ionization and generate additional carriers. The newly generated carriers can also obtain enough energy as they travel through the high electric field to undergo additional impact ionizations. This results in an “avalanche”. The multiplicative gain of a p-i-n design, with a multiplication width of W can be calculated using the following expression (3)

$$M = \left\{ 1 - \int_0^W \alpha \exp \left[- \int_x^W (\alpha - \beta) dx' \right] dx \right\}^{-1} \quad (3)$$

where α and β are spatially dependent [19], due to non-uniformities in either the electric field or changes in the multiplication material itself (e.g. superlattice structures). For an APD with a uniform electric field and ionization rate across the multiplication region, the gain equation (3) simplifies to

$$M = \frac{1 - k}{\exp(-\alpha W[1 - k]) - k} \quad (4)$$

where $k = \beta/\alpha$. Note that when the denominator becomes zero, the gain of the APD becomes infinite. The voltage at which this occurs is called the “breakdown” voltage, and operating above this voltage is called “Geiger-mode”. Single photon sensitivities are reached in Geiger-mode operation. Note that a thicker multiplication region requires less electric field to reach the breakdown condition.

APDs for near-infrared detection typically utilize a separate absorption and multiplication (SAM) structure (Figure 3). A low bandgap material, such as InGaAs, is used as the absorption layer for the near-infrared photons. A large bandgap material, such as InP, is placed next to the absorption layer and is used as the multiplication material. Implicit in this design is proper grading and charge layers in between the absorption and multiplication regions.

This SAM design has the benefit of decoupling the photo-generation and the avalanche processes from each other [25]. A high electrical field is required in the multiplication region to initiate the avalanche process. If this region uses the same material as the low bandgap absorption region, there would be significant tunneling current. A charge layer can be placed between the multiplication p-i-n junction and the absorption region, with the correct doping to balance the fields in the two regions. The electric field profile under different reverse bias voltages is shown in Figure 4(A).

When the initial bias is applied, the voltage is dropped across the p-i-n junction. There is a small electric field in the absorption region, and thus the current is low [Figure 4(B), green line]. When the reverse bias is higher (blue lines), the charge control layer of the p-i-n becomes fully depleted, and there is some electric field in the absorption region.

This document does not include any export controlled technical data. | CLS 45139187 | RTX, Raytheon Technologies proprietary.

This corresponds to a large increase in the current and the voltage where this occurs is called the “punch through” voltage. Further increases in the reverse bias (purple lines) result in further current increases. When the electric field in the multiplication region becomes greater than the breakdown field (red lines), the current becomes infinite. In this operating regime, the device becomes single photon sensitive.

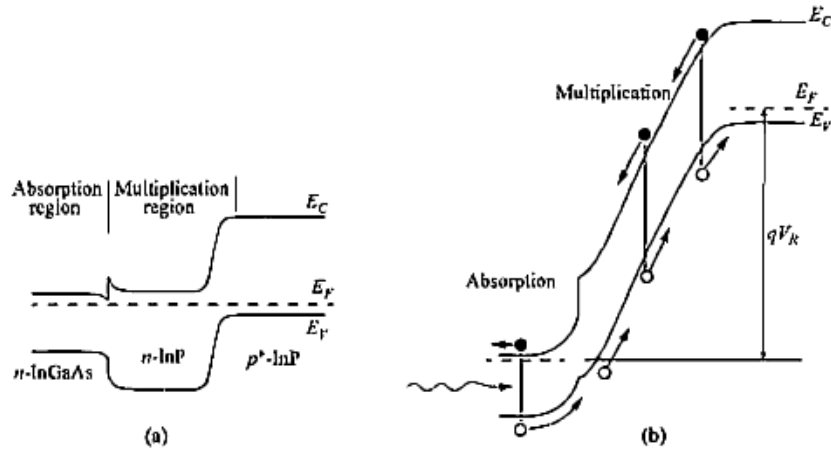


Figure 3. Typical separate absorption and multiplication structure for near infrared APDs, under (a) equilibrium and (b) reverse bias conditions.

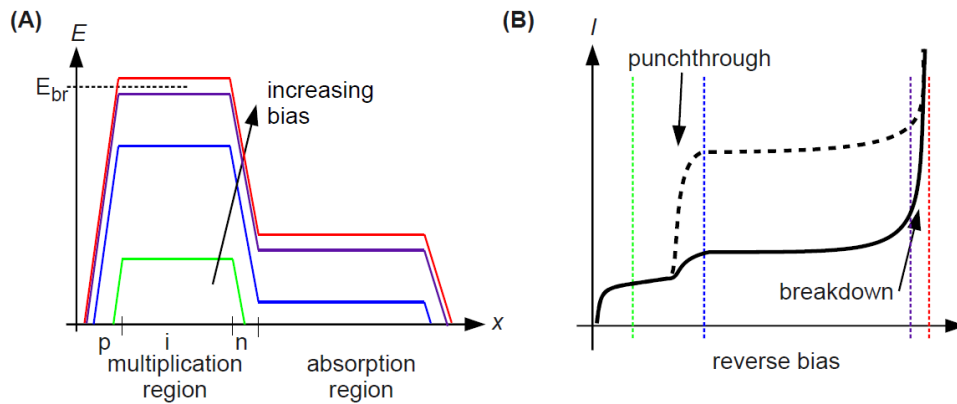


Figure 4. (A) Schematic electric field profile of SAM-APD structure at different reverse bias voltages. (B) Schematic semi-log I-V plot of SAM-APD, under dark (solid) and light (dashed) conditions, with lines depicting the corresponding voltages of the field profile.

In APDs that are biased slightly below the breakdown voltage, photogenerated carriers undergo an impact ionization process, generating avalanche multiplication and a finite gain [26]. APDs that operate in linear/analog mode exhibit maximum useful gain that is limited by strong fluctuations during the multiplication procedure. Thus, APDs operating in this regime are unsuitable for time correlated imaging techniques, where single photon sensitivity and an effective time-gating of the detector are typically required. Instead, APDs can be designed and operated above the breakdown voltage, which is called the Geiger mode of operation [27].

During Geiger mode operation, when a photon is absorbed in the multiplication region of the APD, a self-sustaining avalanche is triggered and the current increases rapidly to a well-detectable level in only picoseconds after the photon was absorbed.

This document does not include any export controlled technical data. | CLS 45139187 | RTX, Raytheon Technologies proprietary.

An external circuit is then needed to quench the multiplication process and restore the APD to its original state, preparing it to detect another photon [28]. The main drawback of APDs with respect to linear mode/analog detectors is the presence of a deadtime after each photon detection which limits the maximum count rate. To bring together the advantages of single-photon detection, typical of GMAPDs, and the photon number resolution, typical of analog detectors, solid-state photodetectors made of GMAPDs operated below breakdown and above breakdown voltage are widely exploited. In addition, the possibility to count each triggered avalanche is achievable both in an analog fashion, where each pixel employs multiple fast resets, integrating every pixel with its own active or passive quenching and amplification/digitization circuitry.

3. INGAAS-BASED APD DEVELOPMENT

Figure 5 shows such a planar detector structure designed using InP/InGaAs material system to operate in SWIR wavelength region of 1000 to 1700nm. In this device structure, the multiplication region consists of undoped InP layer coupled with charge control layer composed of n-type region. These coupled layers provide a high and uniform electric field in the multiplication region. The separated electric field in the multiplication and absorption layers can effectively reduce the band-to-band tunneling and enables the operation of avalanche photodiode at higher gain voltages [29, 30]. This high electric field causes increase in the impact ionization collision rate of both electrons and holes. High electric field in the multiplication region reduces the carrier path length, transit time and avalanche buildup time. The thickness and carrier concentration of the InP charge control layer is optimized keeping the total charge density to be constant for high performance. InGaAsP graded layers mitigate the hole trapping effects due to the abrupt heterojunction band offset between the InP and InGaAs absorption layers. The absorption layer thickness can be optimized to balance the quantum efficiency and the timing response in analog mode. In linear mode, by optimizing the device structure, a gain bandwidth (GBW) product as high as 200 can be achieved with this device structure [31]. To achieve a high gain bandwidth product, a thin multiplication layer width is essential to reduce the avalanche build up time [32, 33]. A thin multiplication layer also has other secondary effects such as enhanced ionization coefficients ratio on high-speed operation of avalanche photodetector [34]. Therefore, one must carefully control the diffusion depth to maintain the thinness of multiplication region.

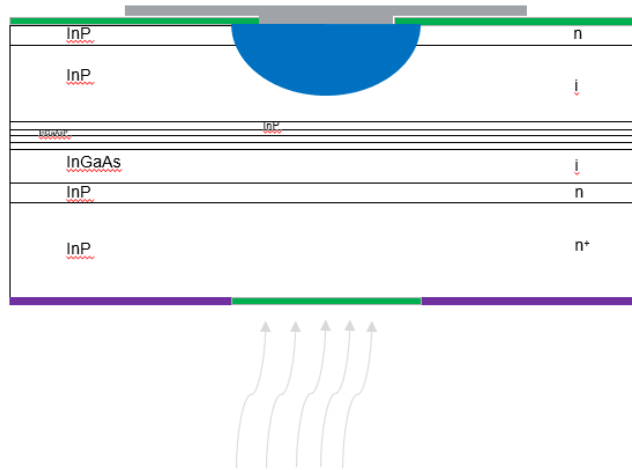


Figure 5. Schematic cross-section of back-illuminated InP/InGaAs avalanche photodiode.

With the precise knowledge of speed of light one can measure a distance by measuring the time that a light pulse needs to travel from an observed target to a reference point. In practice, the active light source and the receiver are co-located. This facilitates a compact setup and avoids shadowing effects.

This document does not include any export controlled technical data. | CLS 45139187 | RTX, Raytheon Technologies proprietary.

A source emits a light pulse and starts a highly accurate counter. The light pulse travels to the target and back. Reception of the light pulse by the detector mechanism stops the counter, which now shows the time of flight of the light pulse. Since the light pulse travels the distance twice (forth and back) a measured time of 6.67 ns corresponds to one meter. An essential property of this setup is the fact that emitter and detector are synchronous. At this point one can recognize a significant advantage of TOF over a triangulation system: the TOF ranging technique does not produce incomplete range data (no shadow effects) because illumination and observation directions can be collinear.

The basic problem of establishing a TOF-ranging system is the realization of the highly accurate, sub-nanosecond counter. There are several methods differing in their needs for illumination source, receiver, and modulation signal. One such TOF distance camera consists of an emitter, infrared or short-wave, that is modulated by a master clock. This modulated light pulse is reflected from the objects in the scene, is collected by the TOF camera's lens and impinges on the image sensor. In each pixel, the sampling/accumulation of generated charge takes place, again controlled by the master clock. After the exposure time, the accumulated charge samples are read out. Since the speed of light in air is precisely known, the phase/time delay is a direct measure of the local distances between the objects in the scene and the range camera. For a wide range of operating conditions, the distance resolution of such TOF range cameras is limited by the photon shot noise and does not depend on electronic noise sources.

4. QUENCHING CIRCUIT DEVELOPMENT

4.1 Discrete Quenching Circuits

The reliability of GMAPDs increased with the introduction of active quenching circuits [35]. By sensing the rise of the avalanche and actively quenching it, these architectures force the quenching and reset operations in relatively short time (few nanoseconds). This innovation ultimately paved the way for single-photon counting and time synchronized single-photon counting applications. Additionally, with the progress in miniaturizing feature sizes in CMOS processes, the supporting finer pitch pixel circuitry and hybridization technologies were also developed [36]. Fully dedicated and flexible fabrication provided best-in-class performance in terms of detection efficiency, noise, and jitter. However, to date, the lack of realizing fine processing control has limited the size of GMAPD arrays to large pitches (25 – 50 μm) and small formats (< 128x128). Improvements in hybridization techniques using modern flip chip technologies enabled the integration of medium-to-large format GMAPD sensor arrays. SUI has fabricated large format (> 128x128) and fine pitch (< 25 μm) GMAPD detector arrays.

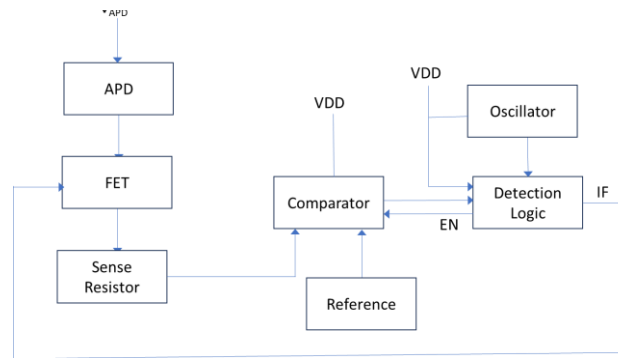


Figure 6. Block diagram showing different components in a typical active quenching circuit.

The main challenge of operating the APD above the breakdown voltage is the subsequent requirements for faster reset or quenching circuitry and for more sensitive and higher dynamic range detection electronics (i.e. be able to absorb photocurrents from few μAs to mAs).

SUI's approach to testing single pixel GMAPD detectors requires a discrete, component-based quenching circuit. A representative quenching circuit block diagram is shown in Figure 6.

This document does not include any export controlled technical data. | CLS 45139187 | RTX, Raytheon Technologies proprietary.

SUI has developed multiple variants: one utilizing a comparator and PMOS FET based discriminator circuit as shown in Figure 7 and the other using a high-speed operational amplifier (OPAMP) and comparator as the voltage discriminator as shown in Figure 8. The comparator and PMOS FET based circuit are limited by the bandwidth of the comparator whereas the OPAMP-based circuit is not. However, the OPAMP-based circuit requires a larger voltage swing to detect the changes at the differential input, which ultimately manifests itself as slower operation. Both variants have shown success towards the characterization of Geiger mode operation of SUI's APDs.

Figure 9 shows the measured dark and photon count rates measured at room temperature. The measured photon count rate is competitive (e.g. > 200 kHz) and is limited by the bandwidth of the comparator. The measured dark count rate is also competitive (e.g. < 200 kHz) for a relatively large (e.g. > 25 μm) diffusion diameter test structure.

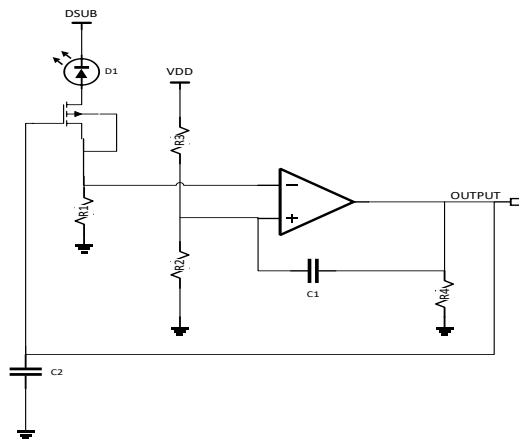


Figure 7. Quenching circuit using a comparator and PMOS FET as a discriminator.

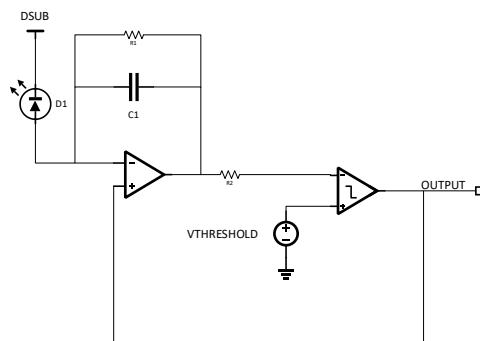


Figure 8. Quenching circuit using the comparator and OPAMP as a discriminator.

The quenching circuits shown in Figures 7, 8 are tantamount to an enhanced passive quenching circuit where the quenching resistor limits the bandwidth and, therefore, the recovery time of the APD. In Figure 10 this limitation has been addressed. In this quenching circuit design the circuit actively modulates a voltage to quench the APD so that it can recover more quickly after avalanche. The circuit generates a pulse of a fixed pulse-width to modulate the quenching voltage, so that the recovery time is fixed for all intensities. For this architecture, when operating the APD in Geiger mode, utilizing higher sense resistor values yields lower dynamic range at the cost of reduced sensitivity. Therefore, careful considerations for selecting this resistor must be made. Additionally, careful timing considerations need to be considered for balancing the APD quenching time with the phase delay of the quenching pulse generation circuitry. This circuitry needs to quench a current on the order of mAs within the pulse width of the returned laser, which is typically < 10s of nanoseconds.

This document does not include any export controlled technical data. | CLS 45139187 | RTX, Raytheon Technologies proprietary.

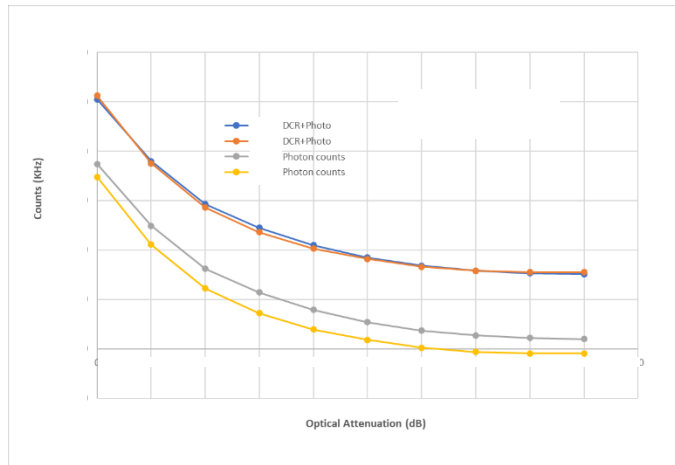


Figure 9. Measured dark and photon count rates of SUI's single element APDs utilizing discrete quenching circuits.

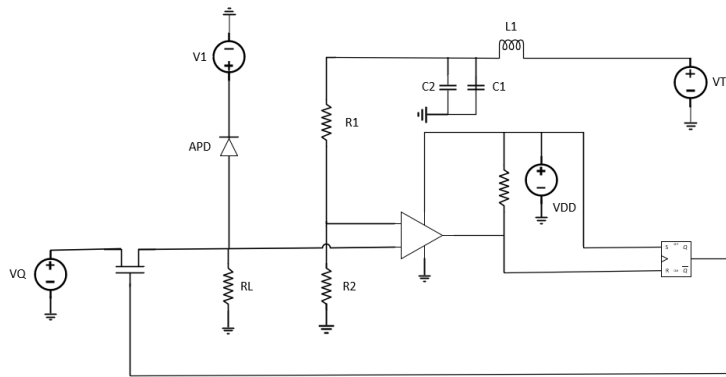


Figure 10. One example of active quenching circuit used to operate SUI's GMAPDs.

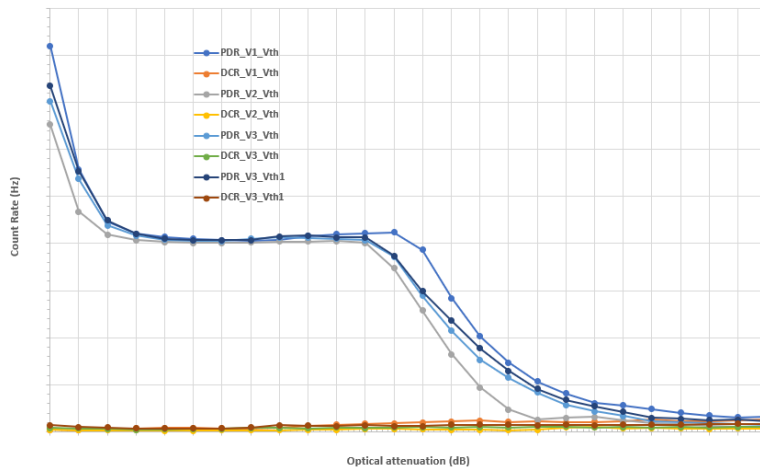


Figure 11. Dark Count Rate (DCR) and Photon Count Rate (PCR) of SUI's GMAPD at various overbias voltages and comparator threshold voltages.

This document does not include any export controlled technical data. | CLS 45139187 | RTX, Raytheon Technologies proprietary.

Figure 11 shows the measured Dark Count Rate (DCR) and Photon Detection Rate (PDR) of SUI's InGaAs/InP APD operating above the breakdown voltage. The DCR is < 200 kHz for all operating voltages and threshold voltages used and the PDR > 200 kHz using a laser source with a pulse width of 10 ns and 200 kHz repetition rate. The intensity is swept down to tens of photons. The dynamic range is demonstrated to be greater than 200 using the quenching circuit shown in Figure 10. The dynamic range can be significantly improved using faster repetition rate and shorter pulse width laser sources.

4.2 CMOS Implementation of Quenching Circuit

The ability to detect single photons is a key capability in an increasing number of applications. Indeed, its scope is not limited to applications that specifically rely on single photons, such as quantum imaging, but also extends to applications where a low signal is overwhelmed by background light, such as in laser ranging applications. Recently silicon-based Single Photon Avalanche Photon Detectors (SPADs) gained popularity because of their small size; their capability to be monolithically integrated with a supporting readout integrated circuit similar to that of PIN-based detectors; their room temperature operation; their relatively low breakdown voltage; and, above all, their capability to be fast-gated (i.e. to time filter the incoming signal), which facilitates precise timestamping of the detected photons. The development of large format, digital pixel arrays, which monolithically integrate the detectors and supporting readout electronics, has allowed the implementation of complex functionality on-chip, tailoring the detectors with optical gain to suit the needs of a given application.

A simple pixel design including passive quenching capability is shown in Figure 12. In this implementation the quenching and amplification/digitization circuitry are implemented at the pixel level in a CMOS ROIC, which is then hybridized with a SWIR GMAPD PDA. The detector operating voltage is adjusted through VQUENCH. The digital output, SPAD_out, of each pixel is conveyed to the readout circuitry. A variant of this circuit is utilized for a portion of the testing results presented in the following section.

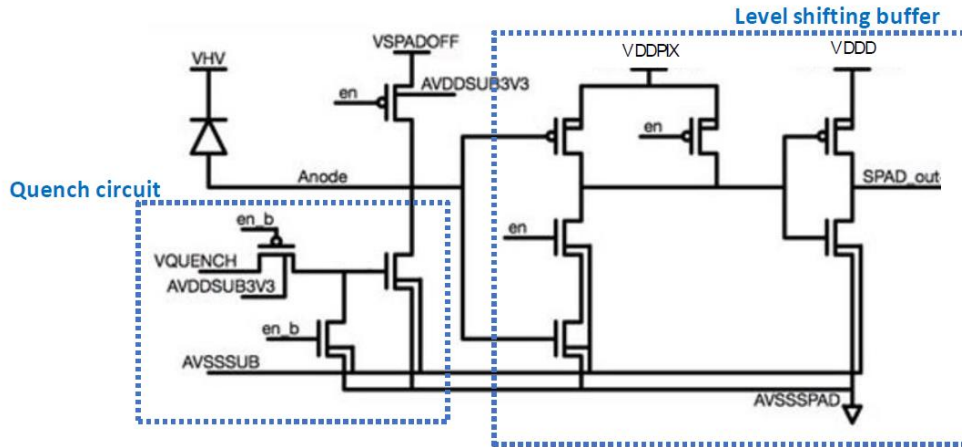


Figure 12. CMOS implementation of in-pixel quenching circuit.

This document does not include any export controlled technical data. | CLS 45139187 | RTX, Raytheon Technologies proprietary.

5. TEST AND CHARACTERIZATION RESULTS

5.1 Measured Single-element GMAPD Performance Using Passive Quenching Circuit

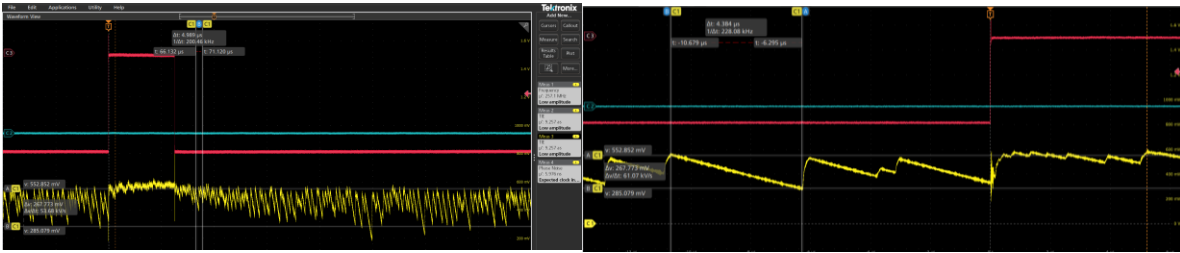


Figure 13. Response of SUI APD operating at an insufficient overbias and excited by a 50 μ s pulse width, 1550 nm laser source. The red trace indicates when the laser source is enabled.

Figure 13 depicts the GMAPD operation of a SUI pixel when operating at insufficient overbias. The results indicate that at these overbias voltages there is a modest increase in the average current, but not enough to initiate true Geiger mode operation. The APD quenches from a peak swing of ~ 270 mV when excited by a 50 μ s pulse width, 1550 nm laser pulse. When the APD is biased here, and when the light pulse is incident on the APD, there is linear increase in the anode voltage of the APD because the APD is still operating in linear mode. In this operating regime, the dark current is significantly higher, which prevents APD from arming. Subsequently, the voltage across the APD is maintained at approximately the breakdown voltage. The APD operates in a similar fashion in the dark.

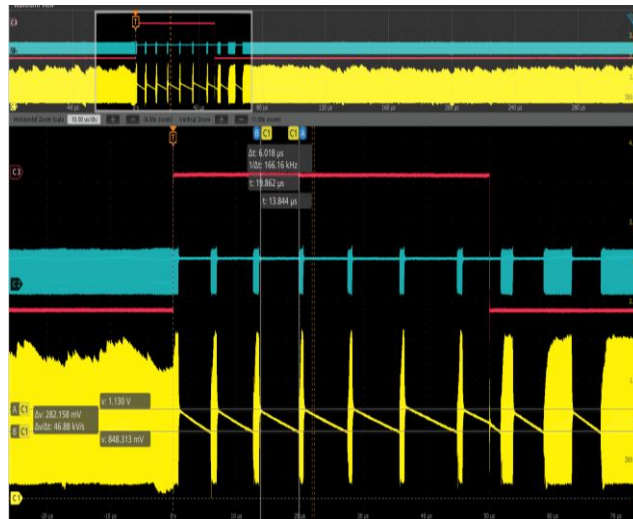


Figure 14. True Geiger mode response of SUI APD operating at a sufficient overbias and excited by a 50 μ s pulse width, 1550 nm laser source. The red trace indicates when the laser source is enabled.

As shown in Figure 14, when the APD is operated at a sufficient overbias, the APD anode voltage decays to 850 mV, triggering the digital threshold of the pixel electronics. This cycle repeats several times with a recovery time of approximately 6 μ s. The dark pulses are negligible as they do not trigger the pixel electronics at this threshold.

This document does not include any export controlled technical data. | CLS 45139187 | RTX, Raytheon Technologies proprietary.

5.2 Wafer-level Testing Results and Comparison with Simulation Results

The key performance parameters of GMAPDs are: Photon-Detection Efficiency (PDE), Photon-Detection Rate (PDR) and Dark Count Rate (DCR). Figure 15 displays these measured performance parameters at the wafer level. In summary, the results indicate when utilizing a 1550 nm wavelength laser that the PDE > 30%, PDR is > 500 KHz and DCR is < 5 kHz. Also, shown in Figure 15 is the measured gain as a function of reverse bias voltage. The measured dark current is in fA range like PIN photodiode current levels at close to zero bias operating voltage (< 100mV) and reaches to pA levels close to the breakdown voltage.

Carriers generated through generation-recombination and tunneling processes within the semiconductor can cause the Geiger-mode avalanche process in the APDs to occur even in the absence of light, producing dark counts even in complete darkness. The average number of counts per second is the DCR of a given device and is a key parameter in determining detector noise.

Before one can measure PDE, PCR, and DCR, the breakdown voltage (V_{BD}) of the pixels in the array must be determined. Once the V_{BD} is determined, then the devices-under-test may be biased appropriately to extract these parameters.

Figure 16 shows the measured dark and photo- current variation as a function of reverse bias voltage. The measured dark and photo- current variation with reverse bias voltage tracks the simulated dark and photo- current variation. Figure 16 shows the measured breakdown voltage variation on a fabricated 3" wafer. As seen from Figure 16, the break down voltage variation is < 3% for the detector structure probed from left-to-right and from top-to-bottom of the wafer. This indicates excellent fabrication process control.

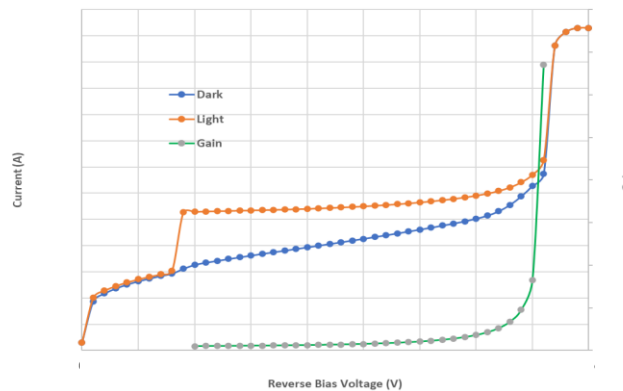


Figure 15. Measured dark and photo current and Gain of a fabricated back-illuminated InP/InGaAs avalanche photodiode pixel.

Figure 17 shows the 2-D and 3-D device cross-section of the simulated back-illuminated planar InP/InGaAs APD. Multiple pixels with a pitch as small as 5 μm were simulated simultaneously to estimate the dark current, responsivity, capacitance and gain as a function operating bias voltage and temperature. In the APD arrays, one of the key performance parameters is the optical crosstalk whereby the avalanche operation in one pixel creates a detectable electrical carrier in the neighboring pixels. One technique to reduce the optical crosstalk is to fabricate the pixels with isolation trenches. Both the planar devices without trenches between the pixels and MESA devices with etched isolation trenches were simulated to understand the crosstalk behavior and hence the detector-level MTF performance. One of the important fabrication process requirements of the planar InP/InGaAsP based APDs is the ability to precisely control the diffusion depth in the avalanche region. The position of the junction in the avalanche region defines the punch-through voltage, the breakdown voltage, and the amount of gain at the dedicated operating voltage.

This document does not include any export controlled technical data. | CLS 45139187 | RTX, Raytheon Technologies proprietary.

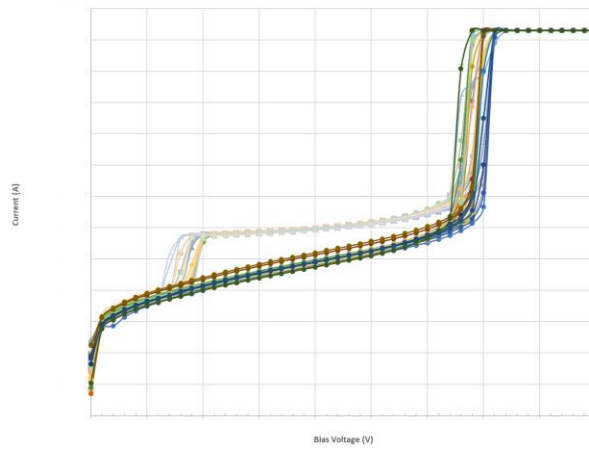


Figure 16. Measured break down voltage uniformity on a 3" wafer.

Figure 18 (a) shows the simulated dark current and photocurrent as a function of reverse bias voltage at 300 K and 260 K. As expected, the breakdown voltage decreases as the temperature decreases from room temperature (300 K) to 260 K. The measured results display a similar decrease in the breakdown voltage. This is shown in Figure 18 (b).

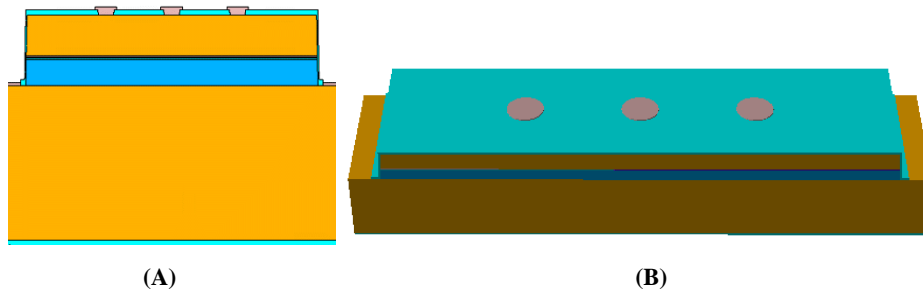


Figure 17. 2-D (A) and 3-D (B) cross-section of back-illuminated InP/InGaAs avalanche photodiode.

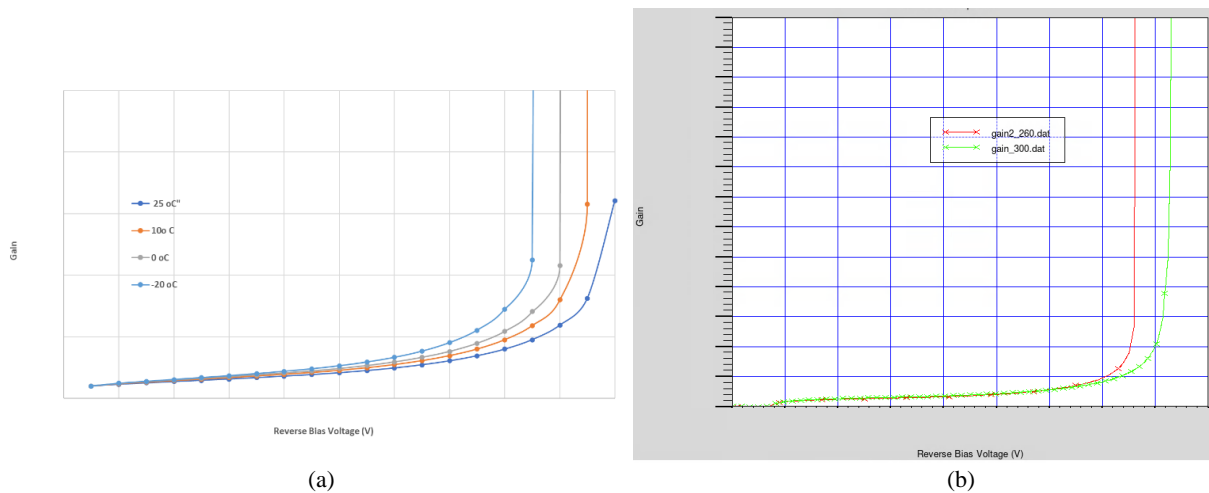


Figure 18. (a) Simulated gain as a function of reverse bias voltage; (b) Measured gain as a function of reverse bias voltage and temperature.

This document does not include any export controlled technical data. | CLS 45139187 | RTX, Raytheon Technologies proprietary.

Figure 19 compares the simulated (a) and measured gain (b) as a function of reverse bias voltage and temperature. The gain increases significantly above the breakdown voltage and reaches $> 1E6$ above breakdown voltage and continue to free run off which forces to bring the bias voltage below break down voltage.

Figure 20 (a) shows the simulated capacitance ($F/\mu m$) of InGaAs/InP APD pixel. The capacitance follows the expected depletion capacitance and agreed with the measured capacitance shape. This indicates precise control of the doping distribution in the depletion layer(s).

Figure 20 (b) displays the optical response uniformity of APD pixel. The response is uniform within the diffusion area of the pixel pitch indicating that there is no edge effect or edge breakdown.

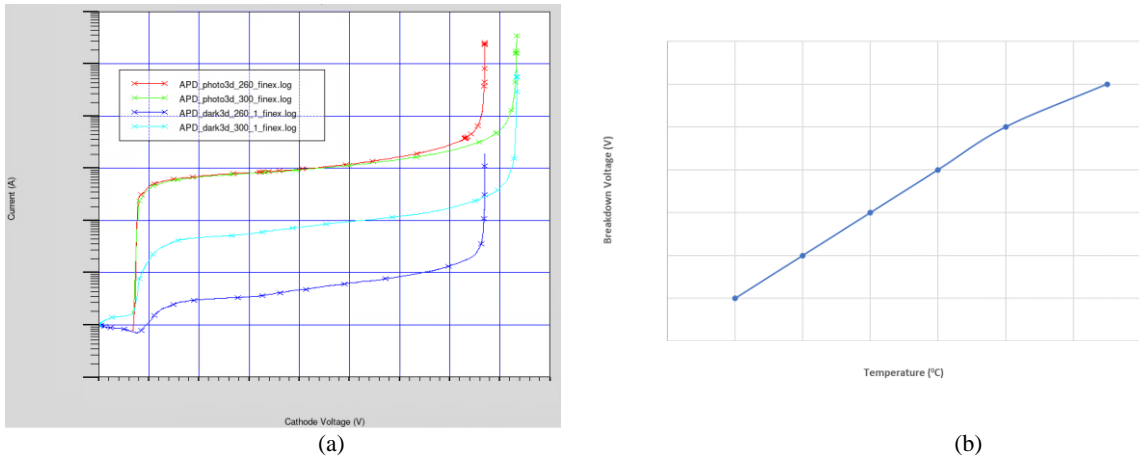


Figure 19. (a) Simulated Dark and Photo current results of InGaAs/InP APD at 300K and 260K; (b) Measured break down voltage variation as function of temperature.

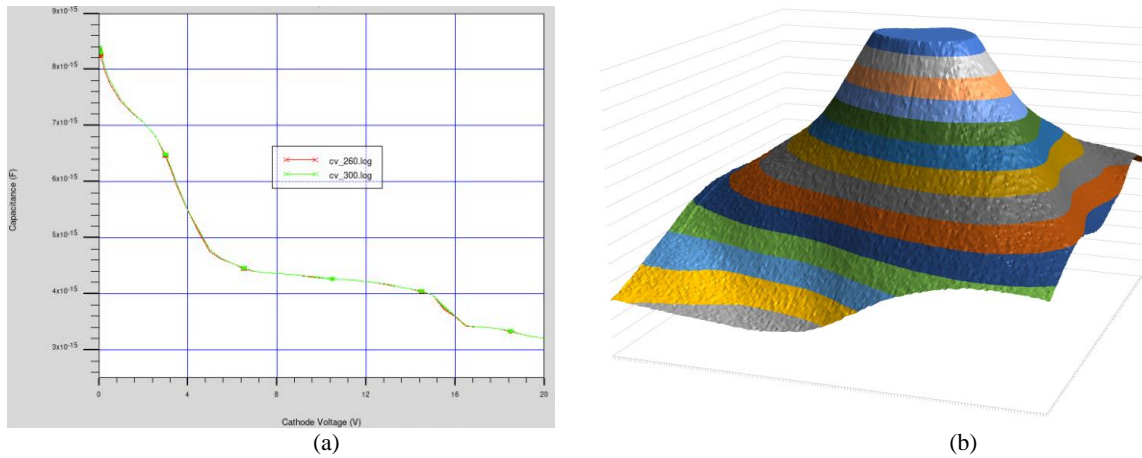


Figure 20. (a) Simulated capacitance vs. reverse bias voltage; and (b) 3-D optical response uniformity both of SUI's InGaAs/InP APD.

6. CONCLUSIONS

This work summarizes recent progress in SUI's 2-D APD development program. Initial results on the integration of 2-D GMAPD arrays with appropriate CMOS pixel with quenching circuit capabilities have been presented. Immediate next steps in this program are not only for the continued improvement and miniaturization of these GMAPDs, but also the development of a full CMOS ROIC and TOF camera development.

ACKNOWLEDGEMENTS

The authors wish to recognize and thank all who contributed to the development of this technology over the years whose names although not explicitly attached here were instrumental in bringing this work to fruition. We would also like to recognize the RTX leadership who entrusted the usage of internal funding to facilitate the work presented within.

REFERENCES

- [1] Y. S. Wang, S. J. Chang, C. L. Tsai, et al. "High-Speed InGaAs PIN Photodetector with Planar Buried Heterostructure," IEEE TRANSACTIONS ON ELECTRON DEVICES, VOL. 56, NO. 6, 1347-1350 (2009).
- [2] Santiago Royo and Maria Ballesta, "An Overview of Imaging Lidar Sensors for Autonomous Vehicles," Appl. Sci. 2019, 9, 4093-4125 (2019).
- [3] Wei Zhang, Michael J. Evans, John C. Lobe, Wei Huang, Paul Bereznycky, et al "Low capacitance SWIR photodetectors for high speed sensing applications" Proc. SPIE 11407, Infrared Technology and Applications XLVI, 114070C (2020).
- [4] Tara Martin, Robert Brubaker, Peter Dixon, Mari-Anne Gagliardi, Tom Sudol, "640x512 InGaAs focal plane array camera for visible and SWIR imaging," Proc. SPIE 5783, Infrared Technology and Applications XXXI, doi: 10.1117/12.603406 (2005).
- [5] US9948880B2 – "Asynchronous multimode focal plane array," 2016.
- [6] US9948880B2 – "Asynchronous multimode focal plane array," 2016.
- [7] US9641781B2 – "Imaging circuit including frame asynchronous pulse detection," 2015.
- [8] Wei Zhang, Paul Bereznycky, Manuel Morales, Wei Huang, Doug Malchow, John Liobe, et al "Fabrication of high aspect ratio bumps for focal plane arrays applications," Proc. SPIE 11002, Infrared Technology and Applications XLV, 110022F (2019).
- [9] Tara Martin, Peter Dixon, Mari-Anne Gagliardi, Navneet Masaun, "320x240 pixel InGaAs/InP focal plane array for short-wave infrared and visible light imaging," Proc. SPIE 5726, Semiconductor Photodetectors II, doi: 10.1117/12.596409 (2005).
- [10] Wei Zhang, Michael J. Evans, Wei Huang, Manuel Morales, Devon Wang, et al "Mesa pixel isolation with low dark current for improved MTF performance in SWIR photodiode array applications," Proc. SPIE 11002, Infrared Technology and Applications XLV, 1100213 (2019).
- [11] K. Taguchi, T. Torika, Y. Sugimoto, K. Makita, H. Ishihara, "Planar-structure InP/InGaAsP/InGaAs avalanche photodiodes with preferential lateral extended guard ring for 1.0-1.6um wavelength optical communication use," IEEE Journal of Lightwave Technology, LT-6, pp. 1643-1988.
- [12] J.C. Campbell, W.T. Tsang, G.J. Qua, B.C. Johnson, "High-Speed InP/InGaAsP/InGaAs Avalanche Photodiodes Grown by Chemical Beam Epitaxy," IEEE Journal of Quantum Electronics, Vol. 24, pp. 496, 1988.
- [13] R. Wang, Y. Tian, Q. Li, Y. Zhao, "High gain and low excess noise InGaAs/InP avalanche photodiode with lateral impact ionization," Applied Optics, Vol. 59, pp. 1980, 2020.
- [14] G. Liu, X. Wang, J. Zhao, W. Chen, Y. Tian, J. Yang, "Modeling a novel InP/InGaAs avalanche photodiode structure: Reducing the excess noise factor," Optics Communications, Vol. 435, pp. 374, 2019.
- [15] Zhang L, Chitnis D, Chun H, Rajbhandari S, Faulkner G, O'Brien D, et al. "A Comparison of APD- and SPAD-Based Receivers for Visible Light Communications." J Lightwave Technol (2018) 36(12):2435–42.
- [16] Guellec F, Tchagaspanian M, "Advanced pixel design for infrared 3D LADAR imaging." Proc. SPIE 6940, Infrared Technology and Applications XXXIV, 69402M (2008). doi: 10.1117/12.779284

- [17] C. Canali, P. Pavan, A. Carlo, P. Lugli, R. Malik, M. Manfredi, A. Neviani, L. Vendrame, E. Zanoni, and G. Zandler, "Experimental and Monte Carlo analysis of impact-ionization in AlGaAs/GaAs HBT's." *Electron Devices, IEEE Transactions on*, volume 43, no. 11 pp. 1769-1777, nov 1996. doi:10.1109/16.542420.
- [18] F. Osaka, T. Mikawa, and O. Wada, "Analysis of Impact Ionization Phenomena in InP by Monte Carlo Simulation." *Japanese Journal of Applied Physics*, volume 25, no. Part 1, No. 3 pp. 394-401, 1986. doi:10.1143/JJAP.25.394.
- [19] D. Harrison, R. A. Abram, and S. Brand, "Impact ionization rate calculations in wide band gap semiconductors." *Journal of Applied Physics*, volume 85, no. 12 pp. 8178-8185, 1999. doi:10.1063/1.370657.
- [20] N. Sano, M. Tomizawa, and A. Yoshii, "Monte carlo analysis of hot electron transport and impact ionization in silicon" *Japanese Journal of Applied Physics*, volume 30, no. Part 1, No. 12B pp. 3662-3666, 1991; doi:10.1143/JJAP.30.3662.
- [21] D. Harrison, R. A. Abram, and S. Brand, "Characteristics of impact ionization rates in direct and indirect gap semiconductors." *Journal of Applied Physics*, volume 85, no. 12 pp. 8186-8192, 1999; doi:10.1063/1.370658.
- [22] M. Saleh, M. Hayat, P. Sotirelis, A. Holmes, J. Campbell, B. Saleh, and M. Teich, "Impact-ionization and noise characteristics of thin III-V avalanche photodiodes" *Electron Devices, IEEE Transactions on*, volume 48, no. 12 pp. 2722-2731, dec 2001. doi:10.1109/16.974696.
- [23] C. A. Armiento, S. H. Groves, and C. E. Hurwitz, "Ionization coefficients of electrons and holes in InP." *Applied Physics Letters*, volume 35, no. 4 pp. 333-335, 1979; doi:10.1063/1.91111.
- [24] L. W. Cook, G. E. Bulman, and G. E. Stillman, "Electron and hole impact ionization coefficients in InP determined by photomultiplication measurements." *Applied Physics Letters*, volume 40, no. 7 pp. 589-591, 1982. doi:10.1063/1.93190.
- [25] L. Tarof, J. Yu, T. Baird, R. Bruce, and D. Knight, "Temperature measurements of separate absorption, grading, charge, and multiplication (SAGCM) InP/InGaAs avalanche photodiodes (APD's)", *Photonics Technology Letters, IEEE*, volume 5, no. 9 pp. 1044-1046, sept. 1993. doi:10.1109/68.257186.
- [26] Zhang L, Chitnis D, Chun H, Rajbhandari S, Faulkner G, O'Brien D, et al. "A Comparison of APD- and SPAD-Based Receivers for Visible Light Communications." *J Lightwave Technol* (2018) 36(12):2435–42.
- [27] Zappa F, Tisa S, Tosi A, Cova S. Principles and Features of Single-Photon Avalanche Diode Arrays. *Sensors Actuators A: Phys* (2007) 140:103–12.
- [28] Tisa S, Zappa F, Tosi A, Cova S. "Electronics for Single Photon Avalanche Diode Arrays," *Sensors Actuators A: Phys* (2007) 140(1):113–22.
- [29] J. Liu, W. Ho, J. Chen, J. Lin, C. Teng, C. Yu, Y. Li, M. Chang, "The fabrication and characterization of InAlAs/InGaAs APD based on a mesa-structure with polyimide passivation," *Sensors*, Vol. 19, pp. 3399, 2019.
- [30] S. Xie, S. Zhang, C. Tan, "InGaAs/InAlAs Avalanche Photodiode with low dark current for high-speed operation," *IEEE Photonics Technology Letters*, Vol. 27, pp. 1745, 2015.
- [31] G. Liu, X. Wang, J. Zhao, W. Chen, Y. Tian, J. Yang, "Modeling a novel InP/InGaAs avalanche photodiode structure: Reducing the excess noise factor," *Optics Communications*, Vol. 435, pp. 374, 2019.
- [32] K. Hyun, C. Park, "Breakdown characteristics in InP/InGaAs avalanche photodiode with PIN multiplication layer structure," *Journal of Applied Physics*, Vol. 81, pp. 974, 1997.
- [33] K. Anselm, H. Nie, C. Hu, C. Lenox, P. Yuan, G. Kinsey, J. Campbell, B. Streetman, "Performance of thin separate absorption charge and multiplication avalanche photodiodes," *IEEE Journal of Quantum Electronics*, Vol. 34(3), pp. 482, 1998.
- [34] M. Hayat, O. Kwon, Y. Pan, P. Sotirelis, J. Campbell, B. Saleh, M. Teich, "Gain-bandwidth characteristics of thin avalanche photodiodes," *IEEE Transactions on Electron Devices*, Vol. 49(5), pp. 770, 2002.
- [35] Cova S, Longoni A, Andreoni A. Towards Picosecond Resolution with Single-photon Avalanche Diodes. *Rev Scientific Instr* (1981) 52(3).
- [36] Cova S, Ghioni M, Lacaíta A, Samori C, Zappa F. Avalanche Photodiodes and Quenching Circuits for Single-Photon Detection. *Appl Opt* (1996) 35(12).